Macromolecules 1992, 25, 1242–1253

Crystalline–Amorphous Block Polypropylene and Nonsymmetric *ansa*-Metallocene Catalyzed Polymerization[1]

Geraldo Hidalgo Llinas,[2a] S.-H. Dong,[2a] Daniel T. Mallin,[2b] Marvin D. Rausch,[2b] Y.-G. Lin,[2c] H. Henning Winter,[2c] and James C. W. Chien*[,2a,b]

Departments of Polymer Science and Engineering, Chemistry, and Chemical Engineering, University of Massachusetts, Amherst, Massachusetts 01003

Received April 8, 1991; Revised Manuscript Received August 22, 1991

ABSTRACT: Propylene has been polymerized with *rac*-[*anti*-ethylidene(1-η^5-tetramethylcyclopentadienyl)-(1-η^5-indenyl)]dichlorotitanium activated with methylaluminoxane. The polypropylene (PP) with T_m of 67–71 °C, soluble in a single solvent and narrow in molecular weight distribution, was shown by dynamic mechanical and elastic measurements to comprise of multiple blocks of stereoregular, crystallizable (cry) PP and stereoirregular, noncrystallizable (am) PP segments, i.e., a thermoplastic elastomer. The molecular structure was estimated from equilibrium modulus, GPC $\bar{M}_n$, and X-ray crystallinity results to be approximately $[(\text{am-PP})_{50}(\text{cry-PP})_{20}]_{30}$ and $[(\text{am-PP})_{100}(\text{cry-PP})_{50}]_{10}$ for the PP's obtained by 25 and 50 °C polymerizations, respectively. The polymers formed at ≤0 °C exhibit no melting endotherm. The stereoregular segments crystallized as a mixture of α- and γ-phases. The results suggest that there may be two isomeric states for the propagation species; chain growth in one state is stereoselective, and it is nonstereoselective in the other state. Frequent isomerization between the two states during the growth of a single macromolecular chain can lead to the formation of thermoplastic elastomeric homopolypropylene.

Introduction

Up until a few years ago, the isospecific polymerization of α-olefin, i.e., propylene, was only achievable with heterogeneous Ziegler–Natta (ZN) catalysts. In 1984, Ewen[3] showed that a homogeneous ZN catalyst, Cp_2TiPh_2/MAO (Cp = η^5-cyclopentadienyl, Ph = phenyl, MAO = methylaluminoxane), could produce polypropylene (PP) at −85 °C temperature of polymerization (T_p) which contained some isotactic order: [mm] = 0.72 and [mmmm] = 0.51. PP's having higher steric purity were obtained with stereorigid chiral *ansa*-metallocene/MAO catalysts.[3-6] These catalysts are able to select and preferentially incorporate one of the two enantiotropic faces (*re* or *si*)[7] of the prochiral monomer. Kaminsky et al.[5a,b] reported that, at T_p = −10 to +20 °C, the *rac*-Et[$IndH_4$]$_2ZrCl_2$ (1)/MAO catalyst (Et[$IndH_4$]$_2$ = ethylenebis(tetrahydroindenyl)) produced 99+% isotactic PP (i-PP).[8] The most common configurational microstructure of anisotactic PP (aniso-PP) obtained with *rac*-Et[Ind]$_2ZrCl_2$ (2)/MAO (Et[Ind]$_2$ = ethylenebis(indenyl)) was said to be of the ...mmmrrmmm...(rr)-type,[3] i.e., a stereochemical insertion error was self-corrected by an enantiomorphic-site control model. The *ansa*-metallocene system has been said by some to be a "well-defined single site" catalyst.

In fact the PP's produced by Et[Ind]$_2ZrCl_2$/MAO and Et[$IndH_4$]$_2ZrCl_2$/MAO are soluble in low-boiling aliphatic hydrocarbons and even ether and acetone,[4] have low melting temperatures (T_m as low as 54 °C for an acetone-soluble fraction), and tend to crystallize in the γ-modification *reversibly*.[9] Such PP having a steric purity considerably lower than the ideal isotactic structure may be referred as anisotactic PP.[4] The above properties would be expected if the a-PP chain contains the configurational microstructure of the ...mmmmrmmm...(r)-type as well as of the (rr)-type. The former can cause inversion of the helix configuration, resulting in a stereoblock copolymer. Furthermore, the results of radio-labeling experiments[4c] showed the presence of at least two different kinds of catalytic species differing in stereoselectivity; the more stereoselective species has 10-fold greater rate constants of propagation (k_p) and chain transfer to MAO (k_{tr}^A). One possibility is that they are chemically distinct species differing for instance in charge (i.e., neutral or cationic complex), oxidation state, or MAO complexation. A second possibility is that the catalytic species has dissimilar catalytic states in dynamic equilibrium.

Manifestation of the second possibility would be subtle and difficult to discern for the common symmetric metallocenes. However, it can be unambiguously demonstrated with an *ansa*-ligand having two dissimilar hapto systems. In this case, if the two propagating states differ in the stereochemical control of olefin insertion and if they interconvert during the growth of a macromolecular chain, then a stereoblock copolymer would be formed. We have synthesized *rac*-[*anti*-ethylidene(1-η^5-tetramethylcyclopendienyl)(1-η^5-indenyl)]$TiCl_2$[10] (3) and found it capable of producing crystalline–amorphous thermoplastic elastomeric polypropylene (TPE-PP).[11]

The central objective of this work was to investigate the structure and morphology of the TPE-PP and the mechanism of production by 1/MAO.

Experimental Section

Synthesis. All chemicals and solvents were purchased from Aldrich. Solvents were purified by standard methods.[12]

1,2,3,4,6-Pentamethylfulvene (4) was prepared by the reaction of 2,3,4,5-tetramethylcyclopent-2-enone with vinylmagnesium bromide in THF according to the procedure of Bensley and Hintz[13] giving a mixture of the desired fulvene and vinyltetramethylcyclopentadiene in a 5:1 ratio. The mixture was not separated for the subsequent synthesis.

The synthesis of 1-(1-indenyl)-1-(2,3,4,5-tetramethylcyclopentadienyl)ethane (5) was as follows. Indenyllithium was obtained by reacting indene (3 g, 25.8 mmol) in 20 mL of diethyl ether with BuLi (1.65 g, 25.8 mmol) at 0 °C. A 10-mL diethyl ether solution of 4 (3.82 g, 25.8 mmol, crude), was cooled to −25 °C, and then the above solution of indenyllithium was added to it dropwise. The mixture was brought up to ambient temperature and stirred for 12 h. Aqueous HCl (12.9 mL of 2 M HCl) was introducd and stirred for 5 h. The organic phase was separated, solvent removed, and the remaining solution distilled under vacuum, collecting the fraction boiling at 130–140 °C (0.1 Torr). The product 5, obtained at 60% yield, was a golden oily isomeric mixture according to ^1H and ^{13}C NMR spectra. Anal. Found (calcd): C, 90.63 (90.85); H, 9.25 (9.15).

0024-9297/92/2225-1242$03.00/0

Table I
Propylene Polymerizations[a] Catalyzed by 1/MAO

	T_p = 25 °C			T_p = 0 °C			T_p = −20 °C		
t_p, min	Δt_p, min	Y,[b] g	$(\Delta Y/\Delta t) \times 10^5$, M s^{-1}	Δt_p, min	Y, g	$(\Delta Y/\Delta t) \times 10^5$, M s^{-1}	Δt_p, min	Y, g	$(\Delta Y/\Delta t) \times 10^5$, M s^{-1}
0.5	0.5	0.015	11.9	0.5	0.025	19.84	0.5	0.04	31.7
1	0.5	0.025	7.93	0.5	0.04	11.9	0.5	0.08	31.7
2	1	0.045	7.93	1	0.06		1	0.10	
3	1	0.065	7.93	1	0.085	9.92	1	0.14	15.8
4	1	0.078	5.15	1	0.11	9.92	1	0.15	
5	1	0.090	4.76	1	0.13		1	0.18	11.9
6	1	0.095	1.98	1	0.142		1	0.20	7.9
7	1	0.100	1.98	1	0.16	7.93	1	0.22	7.9
8	1	0.102	0.79	1	0.175	5.95	1	0.23	3.9
9	1	0.105	–	1	0.187	3.96	1	0.25	
10	1	0.107	0.79	1	0.20	3.96	1	0.26	3.9
20	10	0.120	0.51	10	0.25	1.98	10	0.27	3.9

[a] [3] = 27 μM, [Al]/[Ti] = 2000, $p_{C_3H_6}$ = 1.7 atm, toluene = 100 mL. [b] Yield of PP in g.

The catalyst 3 was prepared as follows. A solution of 5 (2 g, 7.5 mmol, in 20 mL of diethyl ether) was cooled to 0 °C, and *n*-BuLi (15.15 mmol, 6 mL of a 2.5 M solution in diethyl ether) was added dropwise. The mixture was stirred for 12 h at ambient temperature. The white solid product was washed several times with 10 mL of *n*-hexane and then suspended in 15 mL of 2:1 *n*-hexane/diethyl ether. After cooling to −25 °C, a $TiCl_4$·2THF solution (1.42 g, 7.5 mmol, in 10 mL of diethyl ether) was added dropwise and the mixture allowed to react at room temperature for 12 h. The reaction mixture was filtered, and the solvent in the filtrate was removed. The product 3 in 95% green yield was recrystallized from toluene/*n*-hexane. Anal. Found (calcd): C, 62.5 (63.02); H, 5.65 (5.82). ^{1}H NMR spectra ($CDCl_3$): 1.68 (s, 2 H), 1.95 (s, 3 H), 1.96 (s, 3 H), 1.98 (s, 3 H), 2.19 (d, 3 H), 4.96 (q, 1 H), 5.70 (d, 1 H), 6.95–7.59 (m, 5 H). Only one of the two possible diastereomers was obtained by this synthetic method.

If the above synthesis was performed using $TiCl_4$ instead of the $TiCl_3$·2THF complex, then both diastereomers, 3 and 3′, were produced in equal amounts.

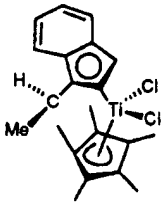

3

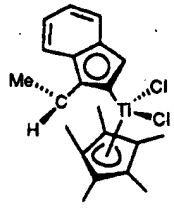

3′

Attempts to grow a single crystal of 3 were unsuccessful. 3 was converted to the dimethyl derivative $MeCH(\eta^5\text{-}C_5Me_4)(\eta^5\text{-}C_9H_6)TiMe_2$ (6).[14] The crystal structure of 6 was found by X-ray diffraction to correspond to 1 which is the anti diastereomer[14] as postulated previously based on steric considerations.[10]

Methylaluminoxane (MAO) was synthesized as follows. Finely pulverized $Al_2(SO_4)_3$·$18H_2O$ (80 g dispersed in 150 mL of toluene) was introduced into a 1-L Schlenk type round-bottomed flask under argon immersed in an ice bath. Neat trimethylaluminum (800 mL, 2 mol) was added dropwise while the reaction mixture was slowly warmed up to 40 °C and stirred for 24 h at that temperature. The inorganic solid was removed by filtration and discarded. The filtrate was evacuated to obtain white MAO solid.

Polymerization and Kinetics. Polymerization was carried out in a 250-mL crown-capped glass pressure reactor with magnetic stirring.[15] Purified toluene (50–100 mL) and MAO were introduced under argon, and the reactor was capped. The reactor was immersed in a constant-temperature bath, evacuated, and saturated with propylene. The solubility of propylene at 1.7 atm in toluene as a function of temperature had been determined to be 0.25, 0.47, 0.73, and 0.94 M at +50, +25, 0, and −20 °C, respectively.[3b] Polymerization began immediately following the injection of the catalyst (20 mg of 3 in 10 mL of toluene). After a desired time interval (t_p), the polymerization was quenched with methanol and the polymer was worked up by standard procedure.[15] From the data of polymer yield (Y) versus t_p, we obtained the rate of polymerization (R_p) as a function of t_p.

The metal–polymer bond concentration ([MPB] = [Ti–P] + [Al–P]) was determined by quenching of the polymerization mixture with CH_3O^3H (24.1 mCi/mol) and radio-assay.[16] The kinetic isotope effect was obtained from the ratio of the maximum specific activity in PP quenched with a near stoichiometric amount of CH_3O^3H (4[Ti] + [Al]) to the constant specific activity in PP quenched with excess CH_3O^3H. The value of the kinetic isotope effect is 1.53, which is similar to the values found for other heterogeneous Ti,[16a,b,d] V,[16f] and homogeneous Zr[4c,16c,e] ZN catalyst systems. The polymers obtained at a particular T_p are denoted as PP(T_p).

Polymer Characterization. Number- and weight-average molecular weights, $\bar{M}_n$ and $\bar{M}_w$, were obtained with a Waters 150C GPC instrument. The columns were calibrated with polyethylene standards. The GPC $\bar{M}_w$ values were found to be in close agreement with the light-scattering-determined values.[4b] The intrinsic viscosity ([η]) of PP was measured in decalin at 135 °C using an Ubbelohde viscometer.

PP was placed in a Kumagawa apparatus and extracted[17] with refluxing solvents of descending polarity and ascending boiling points in the order acetone, diethyl ether, *n*-pentane, *n*-hexane, and *n*-heptane. The fractionated polymer was recovered by evaporation of the solvent.

Dynamic mechanical measurement was made on a Rheometrics dynamic spectrometer (RDS Model 7700) using a cone/plate geometry. The sample was molded in the rheometer usually at 75 °C but also at higher temperatures for some specimens. The sample for mechanical elastic property measurement was molded at 120 °C into a dogbone shape with 20 × 5 × 0.5 mm^3 for the extension part. After being cooled to ambient temperature, the specimen was stored for 3 days prior to the mechanical tests. The specimens were extended at 20 cm/min, using an Instron Model TTBN tensile machine.

A Siemens D-500 diffractometer was used to obtain powder patterns by using a Ni-filtered Cu Kα X-ray beam excited at 40 kV. A Perkin-Elmer System IV instrument was used to obtain a DSC melting endotherm. The DSC procedures are detailed in the Results section.

Results

Polymerization Kinetics. Propylene polymerizations catalyzed with [3] = 27 μM and [Al]/[Ti] = 2000 were quenched after various times. The yields, given in Table I for T_p = +25, 0, and −20 °C, are plotted versus t_p in Figure 1. The variations of the rate of polymerization (R_p) versus t_p are shown in Figure 2. The decay of R_p was precipitous at T_p = 50 °C, so R_p cannot be measured with accuracy. The decay became more gradual as T_p was lowered.

The polymers quenched with CH_3O^3H were radio-assayed to determine [MPB] from the measured specific activity. Figure 3 contains the plots of [MPB] versus po-

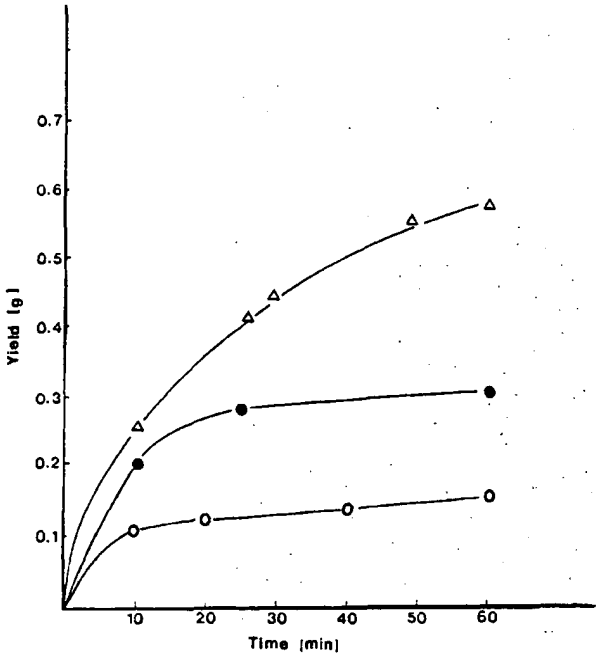

Figure 1. Yield versus time of propylene polymerizations catalyzed by 1/MAO with [3] = 27 μM, [Al]/[Ti] ≈ 2000, 100 mL of toluene, $p_{C_3H_6}$ = 1.7 atm, and T_p at (○) +25 °C, (●) 0 °C, and (△) −20 °C.

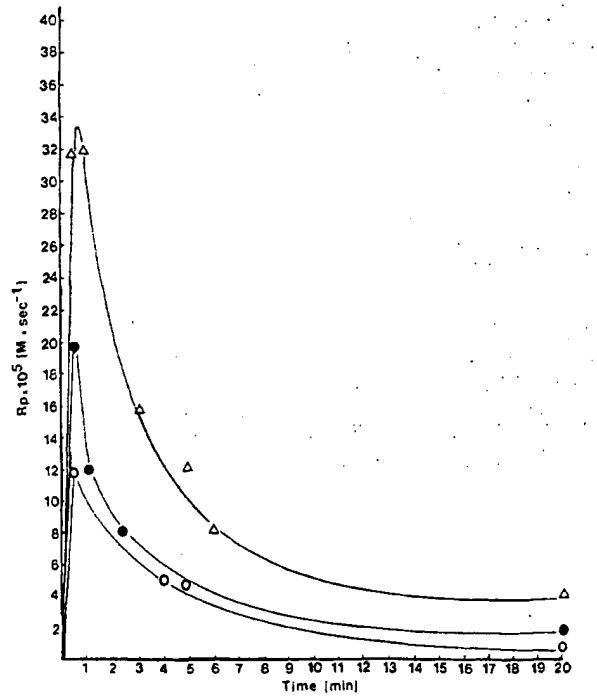

Figure 2. R_p versus time plots of the data in Figure 1.

lymerization yield (Y). The intercept at $Y = 0$ gives the initial and maximum concentration of [Ti–P], which is taken to be the initial concentration of the active species, $[C^*]_0$. The values of $[C^*]_0$ were found to be 3.7, 4.25, and 3.7% of 3 for T_p at −20, 0, and +25 °C, respectively. The value of k_p was obtained from

$$k_p = R_{p,m}/[C^*]_0[C_3H_6] \qquad (1)$$

[MPB] increases with t_p due to the transfer of a propagating chain from Ti to MAO. The value of this rate constant (k_{tr}^A) can be calculated from the slope of the linear plot in Figure 3.

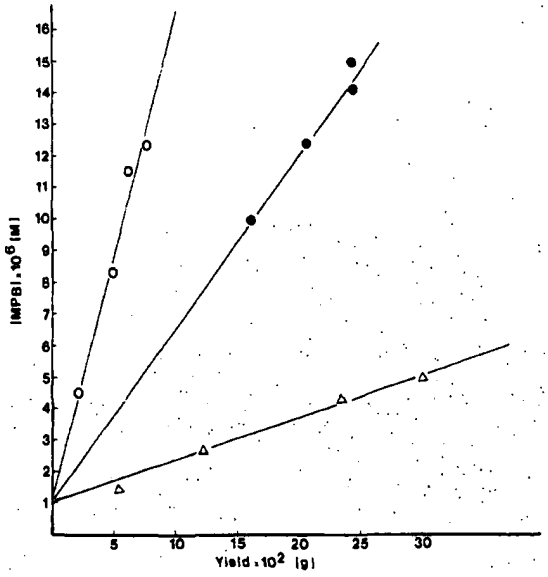

Figure 3. Variation of [MPB] versus polymerization yield (Y) at T_p: (○) +25 °C; (●) 0 °C; (△) −20 °C.

Table II
Kinetic Data for Propylene Polymerization

T_p, °C	$[C^*]_0$ % of I	k_p, $(M\,s)^{-1}$	$k_{tr}^A \times 10^2$, s^{-1}	$k_d \times 10^3$, s^{-1}	(k_{tr}^β), s^{-1}
25	3.7	211	1.5	5.7	(0.04)
0	4.25	236	0.9	4.4	(0.09)
−20	3.7	362	0.4	3.8	

Table III
Variation of MW of PP with Time of Polymerization

T_p, °C	t_p, min	$[\eta]$, dL/g	$\bar{M}_v \times 10^{-5}$
25	10	0.69	0.63
	30	0.63	0.56
	60	0.75	0.70
0	10	0.58	0.51
	30	1.0	1.0
	60	1.30	1.39
−20	10	2.4	2.99
	30	2.6	3.30
	60	3.25	4.66

$$[MBP]_t = [MBP]_0 + \frac{k_{tr}^A}{k_p[C_3H_6]}Y \qquad (2)$$

The results of these kinetic parameters are summarized in Table II.

The intrinsic viscosity was determined on PP samples quenched at various t_p. Table III gives this change of $[\eta]$ as a function of t_p at different T_p. Values of $\bar{M}_v$ were calculated by the equation

$$[\eta] = 10^{-4}[\bar{M}_v]^{0.8} \qquad (3)$$

developed for monodisperse PP fractions[18] and plotted in Figure 4. The PP obtained at 25 °C has the lowest $\bar{M}_v$ and is independent of t_p. Polymerization at −20 °C produced PP having the highest $\bar{M}_v$, and its $\bar{M}_v$ increases with t_p.

Polymer Compositions and Molecular Weights. The PP was fractionated by a classical solubility separation technique.[18] The 25 and 50 °C products, designated respectively as PP(25) and PP(50), are completely soluble in diethyl ether (Table IV). At lower T_p there was produced diethyl ether insoluble polymers. The amounts

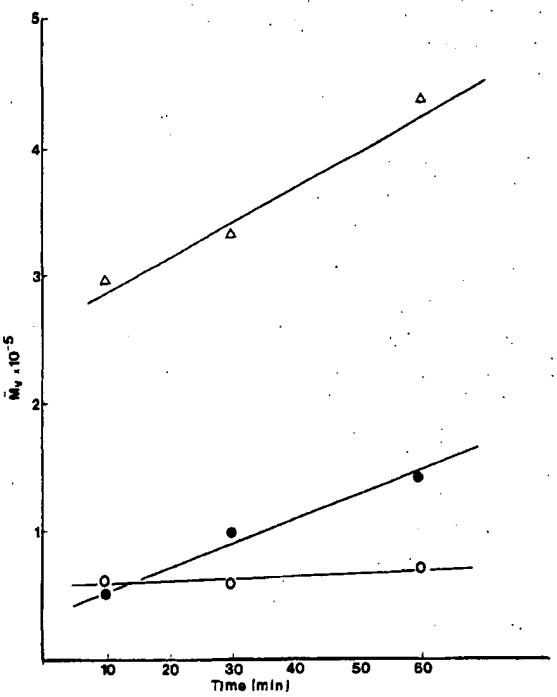

Figure 4. Variation of $\bar{M}_v$ versus time of polymerization at T_p: (○) +25 °C; (●) 0 °C; (△) −20 °C.

Table IV
Fractionation of PP

	wt % of PP soluble in			
T_p, °C	diethyl ether	pentane	hexane	heptane
50	100			
25	100			
0	40.9	51.2	7.9	
−20	17.3	54.4	29.2	4.1

Table V
Polypropylene Molecular Weights and Distributions Determined by GPC

T_p °C	$\bar{M}_n \times 10^{-5}$	$\bar{M}_w \times 10^{-5}$	PD[a]
0	1.04	2.13	2.06
0	1.01	2.19	2.16
25	0.98	1.64	1.67
25	0.97	1.74	1.81
50	0.66	1.27	1.91
50	0.63	1.17	1.86

[a] PD = $\bar{M}_w/\bar{M}_n$.

of pentane (C_5), hexane (C_6), and heptane (C_7) fractions increase with the decrease of T_p.

$\bar{M}_n$, $\bar{M}_w$, and PD (=$\bar{M}_w/\bar{M}_n$) were determined by GPC for the PP's. The results of duplicate measurements are found in Table V; the deviations are less than ±5% for the duplicates. The observed polydispersity (PD approximately equal to 2) is consistent with the most probable molecular weight distribution.

Dynamic Mechanical Properties. The effect of heating on the complex modulus (G^*) of PP's obtained at different T_p is shown in Figure 5. The G^* of PP(50) and PP(25) both decay by about 2 orders of magnitude around 65 °C corresponding to the melting transition of the crystalline domain by DSC (vide infra). In contrast, PP(0) and PP(−20) did not display a similar drop in G^*; they also exhibit not DSC melting transition. The complex modulus in the melt state at elevated temperature is greatest for PP(−20); it decreases for PP obtained at increasing T_p. This trend is in accord with the fact that

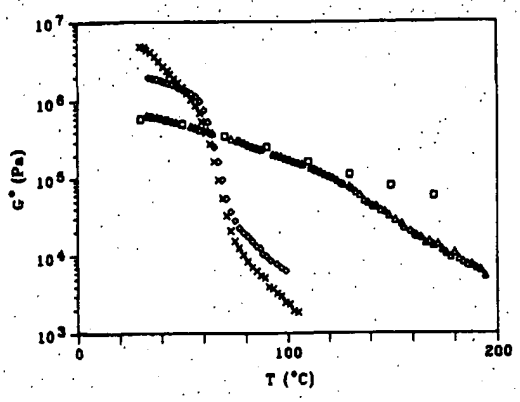

Figure 5. Complex modulus G^* in small-amplitude oscillatory shear (ω = 1 rad/s) of PP(50) (×), PP(25) (◇), PP(0) (△), and PP(−20) (□) during a temperature sweep with a heating rate 1 K/min.

higher T_p leads to a lower number-average degree of polymerization ($\overline{DP}_n$) and that the G^* of a polymer melt scales with molecular weight. The G^*–T_p relationship measured at temperatures below 50 °C exhibits the opposite trend; it is highest for PP(50) and decreases for PP obtained at decreasing T_p. This is probably due to differences in the number and strength of crystalline network junctions.

Changes of the storage modulus (G') and the loss modulus (G'') with temperature are shown in Figure 6. The melting transition caused the lowering of G' and G'' values by 2 and 1 orders of magnitude for PP(50) and PP(25), respectively.

Figure 7 contains the data of the frequency dependences of G' and G'' at low and high temperatures. It shows $G' > G''$ at 50 °C. Both moduli decreased only slightly with the decrease of frequency and leveled off to plateau values at low frequency. PP(25) exhibits a smaller temperature dependence than PP(50) at low temperature, suggesting that the physical network structures are more thermally stable in the former. Above the T_m both TPE's have $G'' > G'$; they decrease monotonically with the decrease of frequency without a plateau at low frequency. This liquidlike dynamic spectra indicates the absence of microphase separation in the melt state; i.e., the crystallizable and noncrystallizable blocks are compatible. The above behaviors are typical for a physically cross-linked TPE. In the case of PP(25) the 90 °C dynamic spectrum at frequencies lower than 1 rad/s shows

$$\text{d log } G'/\text{d log } \omega = 2 \quad \text{and} \quad \text{d log } G''/\text{d log } \omega = 1 \quad (4)$$

for a homogeneous liquid state.

PP(0) behaves differently from the above polymers. It does not have a low-frequency plateau of the storage modulus at 50 °C (Figure 7C), indicating the absence of a three-dimensional physical network. On the other hand, time-temperature superposition is not applicable to the dynamic spectra recorded at 50 and 120 °C. This implies that there is a small amount of a crystalline fraction which melts in this temperature range but is not sufficient to be observed in the temperature sweep curve (Figure 5c).

The dynamic spectra of PP(−20) follow perfectly the time–temperature superposition.[19] The master curve in Figure 8 exhibits an upper rubber plateau. The level of this rubber plateau is determined by the critical molecular weight for physical entanglement and represents the lower limit for the modulus attainable by an elastomeric PP.

The equilibrium shear modulus (G_e) was determined through stress relaxation of a step strain which was 2%

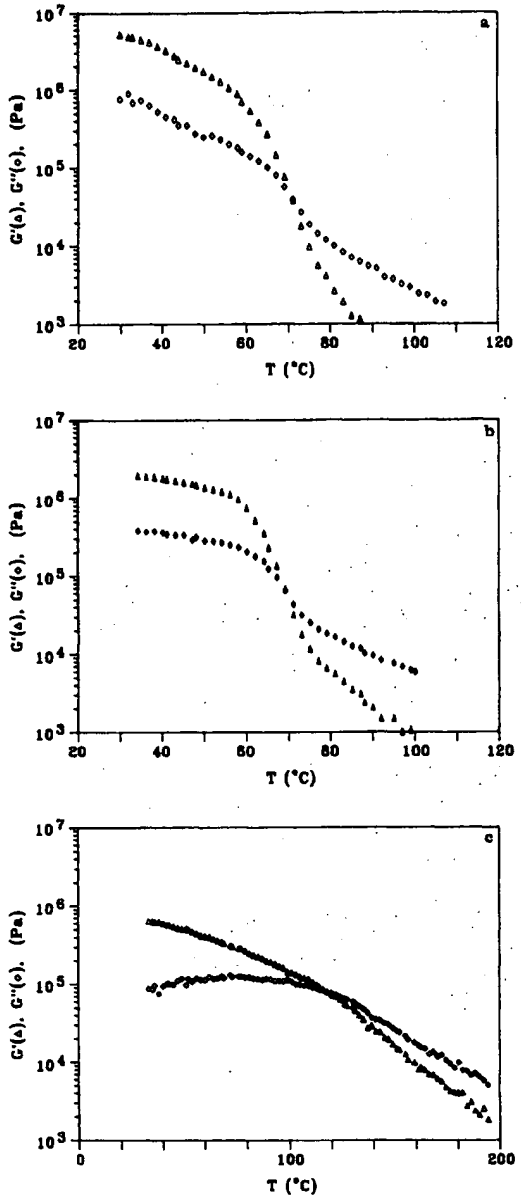

Figure 6. Evolution of storage modulus G' and loss modulus G'' during the temperature sweep at 1 rad/s and a heating rate 1 K/min: (a) PP(50), (b) PP(25), (c) PP(0).

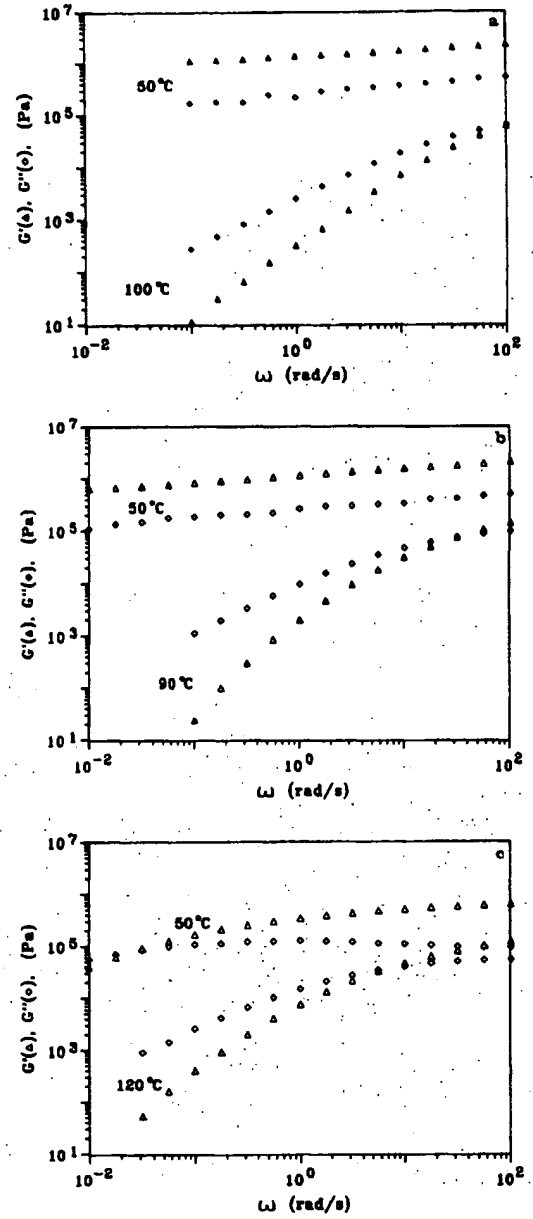

Figure 7. Frequency sweeps at small strain amplitude of (a) PP(50), (b) PP(25), and (c) PP(0) at the indicated temperatures.

of a shear unit. The G_e was reached in a few hundred seconds and has values of 1.16 and 0.56 MPa for PP(50) and PP(25), respectively.

Mechanical Elastic Property. The typical tensile stress curves obtained with an Instron testing machine are given in Figure 9. PP(50) and PP(25) do not display a yield point; their elongations to break at 530% and 1300%, respectively. This behavior is consistent with cross-linked elastomers; the PP(25) is mechanically stronger than PP(50). The tensile curve for PP(0) is characterized by very low tensile modulus, a yield point around 200% elongation, and nearly 2000% elongation to break. These behaviors are typical of non-cross-linked elastomers.

The elasticity of the TPE-PP was characterized by two methods. In the first method, the sample was subjected to 100%, 200%, or 300% elongation, tensile stress was reduced to zero, and then the specimen length was measured after 1 h of recovery. The percentage of recovery is $[(L_1 - L_2)/(L_1 - L_0)] \times 100]$, where L_0, L_1, and L_2 are the sample lengths before stretching, at maximum elongation, and after recovery, respectively. The results are given in Table VI, which also includes the tensile properties.

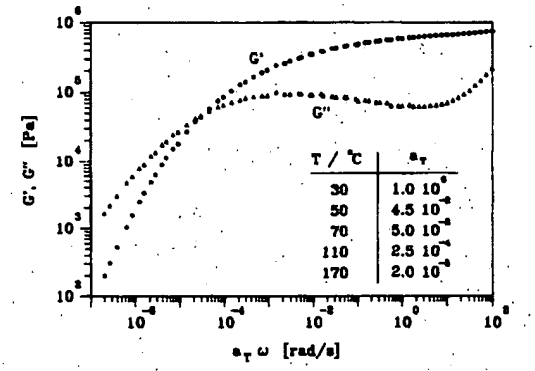

Figure 8. G', G'' master curve of PP(−20) obtained by time–temperature superposition.

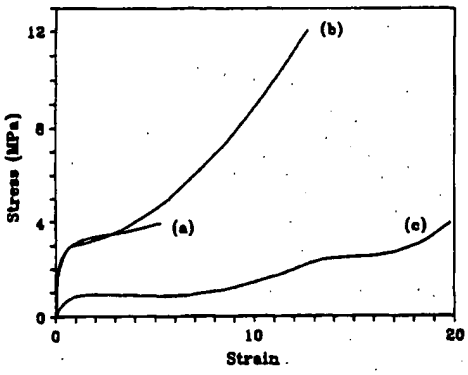

Figure 9. Tensile stress curves of (a) PP(50), (b) PP(25), and (c) PP(0) at room temperature and an elongation rate of 1000%/min.

Table VI
Tensile and Elastic Properties of Polypropylenes

sample	PP(50)	PP(25)	PP(0)
stress at 100% elongation, MPa	3.13	3.07	0.85
recovery after 100% elongation, %	93	97	90
stress at 200% elongation, MPa	3.39	3.30	0.93
recovery after 200% elongation, %	91	96	86
stress at 300% elongation, MPa	3.53	3.59	0.91
recovery after 300% elongation, %	83	92	81
tensile strength, MPa	3.97	12.1	3.96
elongation to break, %	530	1300	2000

In the second method, tensile stress was recorded as the sample was subjected to a series of extension and recovery. This was done by stretching the specimen at 20 cm/min to a desired strain and then reversing the direction when the tensile stress relaxed to zero. Figure 10 shows excellent recovery for PP(25), good recovery for PP(50), but poor recovery for PP(0). This shows that the PP(25) has the strongest physical cross-links among the three materials.

Crystallization. The rate of crystallization for a supercooled TPE-PP is slow as shown by DSC and dynamic mechanical measurements. In these experiments PP(50) was preheated to 100 °C, immediately cooled to 40 °C, and held there for time t_c to allow isothermal crystallization. The moduli G' and G'' increased due to crystallization (Figure 11), but they had not reached plateau values even after 2 h, indicating incomplete crystallization. The crystallization rate at 40 °C was more rapid for PP(25) as shown by the change of G', G'', and tan δ with t_c in Figure 12. Figure 13 presents the data of frequency sweeps at various t_c. At $t_c = 0$, the sample is a simple viscoelastic liquid as explained above. At $t_c = 80$ min both G' and G'' exhibit power law dependence in frequency. This is the gel point which corresponds to the critical point of a liquid/solid transition; it is characterized by the unique phase angle and the power law relationship between moduli and frequency. Our detailed study of crystallization-induced gelation of the TPE-PP has been described elsewhere.[20] For longer t_c, the storage modulus developed a low-frequency plateau, indicating that the sample has become a viscoelastic solid.

Crystallization of TPE-PP was also investigated by DSC. Figure 14 shows the changes of endotherm with t_c. For a short isothermal crystallization time of 10 min, there was a small peak at 68 °C probably due to incomplete melting of the crystalline domains during the first heating to 100 °C. As t_c increases the peak grows in size; the peak maximum initially shifted to a lower t_m of 63 °C and then returned to 68 °C. Figure 15 shows that the increase of the enthalpy of fusion (ΔH_f) with t_c for PP(25) is sigmoidal, indicating a nucleation period followed by crystal growth.

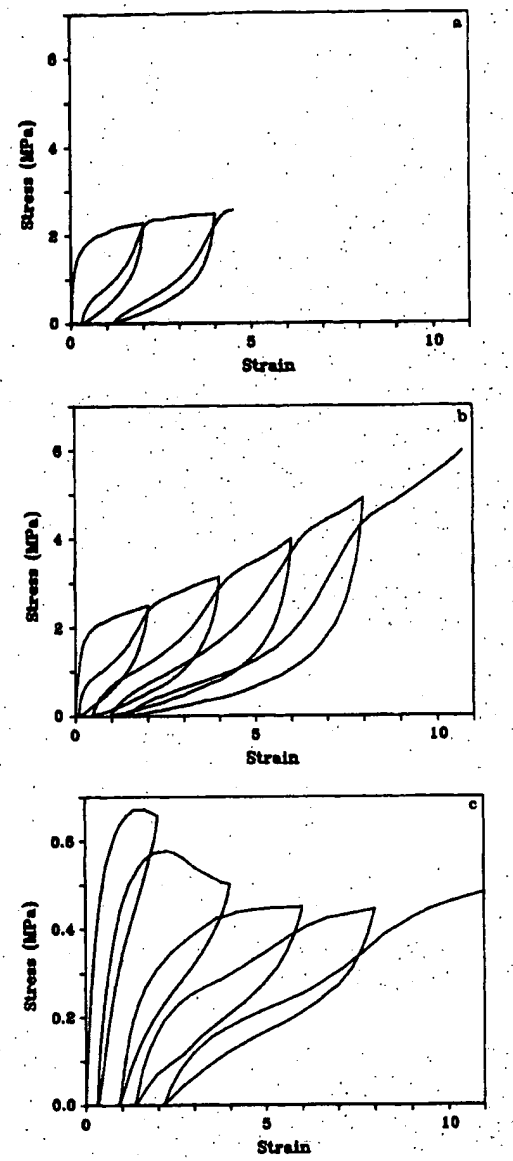

Figure 10. Tensile stress during a series of extension/recovery cycles with a deformation rate ±100%/min: (a) PP(50), (b) PP(25), and (c) PP(0). Note that c is plotted in smaller scale.

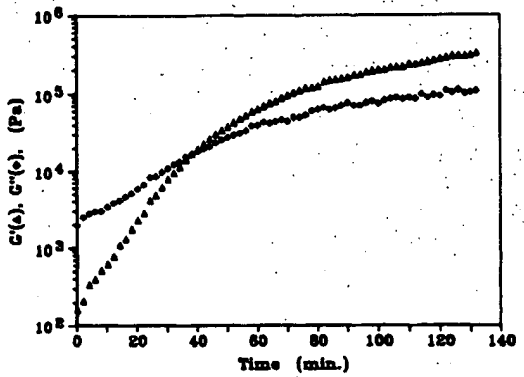

Figure 11. Dynamic moduli (ω = 1 rad/s) of PP(50) during isothermal crystallization at 60 °C. The sample was first heated to 100 °C and then rapidly cooled to 60 °C.

Morphology. The X-ray diffractograms for the PP's are given in Figure 16. The PP(0) sample displays only

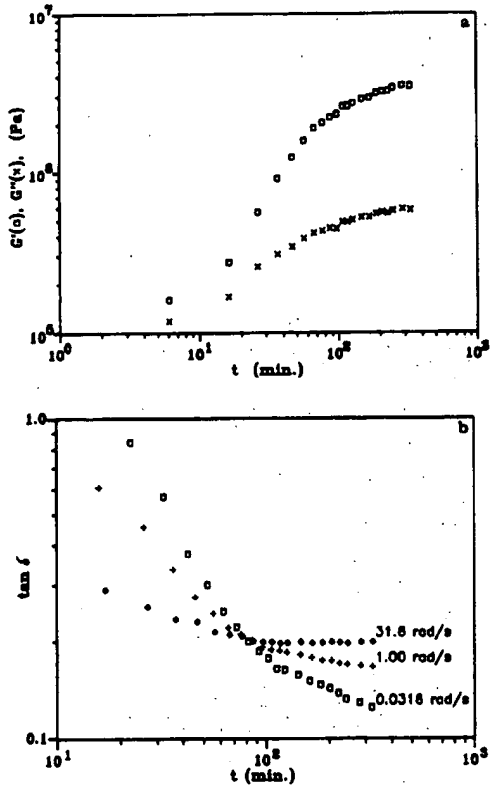

Figure 12. Evolution of (a) mechanical dynamic moduli at 1 rad/s and (b) the loss tangent at the indicated frequencies during crystallization of PP(25) at 40 °C after radpidly cooled from 100 °C. (□) G'; (×) G''.

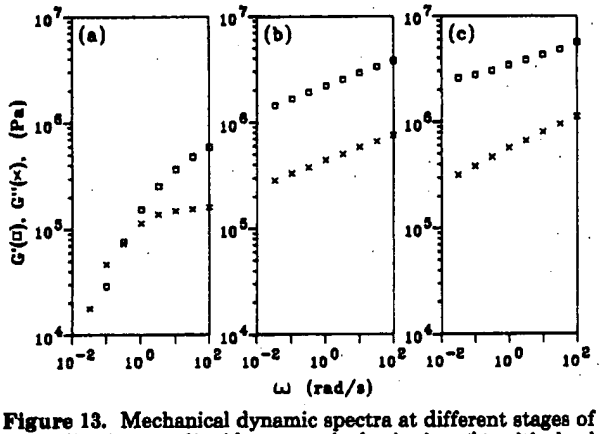

Figure 13. Mechanical dynamic spectra at different stages of crystallization: (a) liquid state at the beginning, (b) critical gel state in 80 min, and (c) solid state in 320 min. The PP(25) sample had been heated to 100 °C before isothermal crystallization at 40 °C. (□) G'; (×) G''.

an amorphous halo, in agreement with the absence of a melting transition by dynamic mechanical (vide supra) and DSC (vide infra) measurements. PP(25) and PP(50) exhibit low crystallinity. The simple method of connecting the minima in the diffraction pattern to obtain $I_c(s)$ from I(s), the crystalline and total scattering intensities, respectively, cannot be used. Instead a resolution function[21]

$$I = F_i H_i \exp\left[-\frac{\ln 2(x-P_i)}{W_i}\right] + \frac{(1-F_i)H_i}{1+4(x-P_i)/W_i} \quad (5)$$

where F_i, H_i, P_i, and W_i are the peak factor, height, position, and width, respectively, for the ith peak, was used to fit all the peaks after first applying the usual corrections for

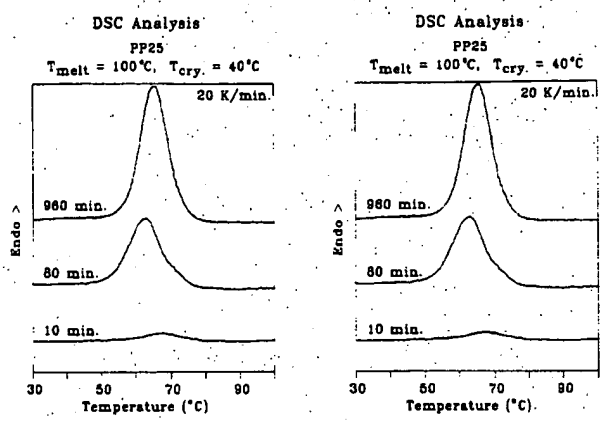

Figure 14. DSC variation with time of isothermal crystallization for (a) PP(25) and (b) PP(50).

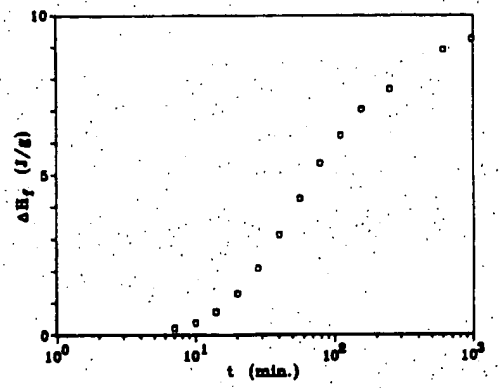

Figure 15. Fusion heat of PP(25) after crystallization at 40 °C for various times. The preheating temperature was 100 °C.

air and Compton scattering, absorption, and polarization. The error of fitting, $[\sum(I(2\theta) - I_{ob}(2\theta))^2/\sum I_{ob}^2(2\theta)]$, was 4.5%. Analysis of the diffractograms of all the samples led to the same F and P parameters (Table VII). The peak widths are greater for the PP(25) and PP(50) polymers than for PP(0). This means a broader distribution of short-range order for the amorphous segment in the presence of crystalline domains than in the absence of them. Roland analysis of the data afforded X_c.

The crystalline diffraction components in parts a and b of Figure 16 showed the presence of both α- and γ-phases as observed previously in the aniso-PP produced by the Et[Ind]$_2$ZrCl$_2$/MAO catalyst.[4b] Both the percent crystallinity (X_c) and the fraction of the γ-phase $X_\gamma = A_{\gamma(1\bar{2}0)}/(A_{\alpha(130)} + A_{\gamma(1\bar{2}0)})$ (A is the peak area) are sensitive to thermal history. Therefore, specimens were kept at an annealing temperature (T_a) for 24 h to promote crystallization. X-ray diffraction was either performed immediately after the sample was cooled to room temperature or 24 h later. The degree or crystallinity (X_c) and percent γ-phase (X_γ) of PP(25) annealed at 30 or 45 °C have comparable values (Table VIII). The sample of PP(50) annealed at 45 °C has a greater X_c than those annealed at 30 and 60 °C, and there is a gradual *increase* of X_γ with the increase of T_a. Storage of the annealed sample at room temperature for 44 h did not change either X_c or X_γ.

The crystallite size $L(hkl)$ can be calculated from the linewidth at half peak height

$$L(hkl) = 0.89\lambda/\beta \cos\theta_{hkl} \quad (6)$$

Instrument broadening was corrected by subtracting the half peak width of hexamethylenetetramine according to the Gauss form. The crystallite size in the b-direction

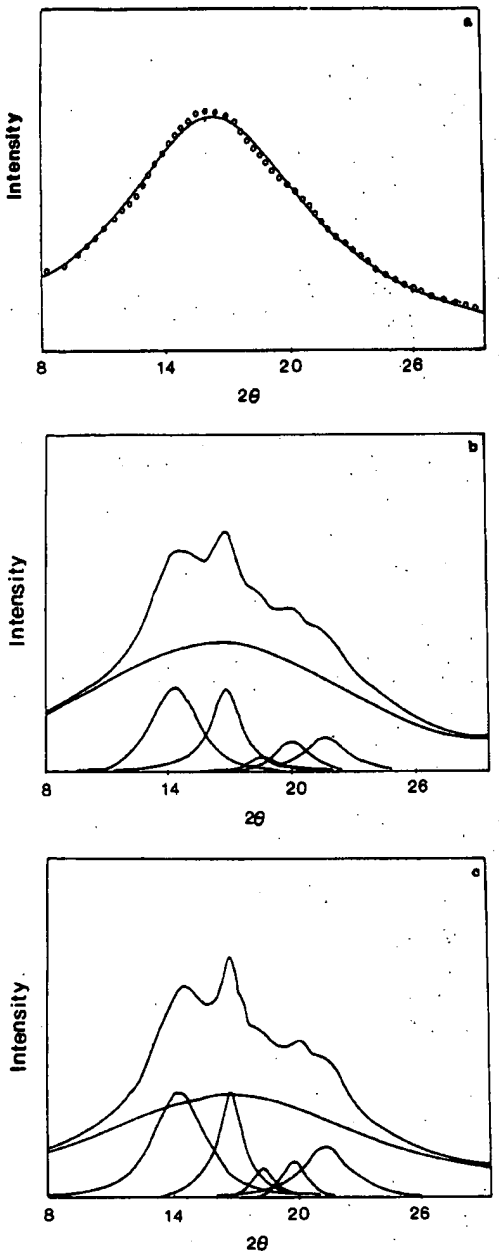

Figure 16. X-ray diffractograms for (a) PP(0), (b) PP(25), and (c) PP(50).

Table VII
Parameters for the Gause and Cachy Resolution Function

sample	F	$P(2\theta)$	W, deg
PP(0)	0.0013	16.21	11.01
PP(25)	0.006	16.61	16.71
PP(50)	0.001	16.81	15.91

was estimated from the (040) and (020) reflections of the α- and γ-phases, respectively. Values of L in the c-dimension were obtained using the (041) peak corrected by $L(c\text{-axis}) = L(041)\cos\theta_0$ ($\cos\theta_0 = 51.8°$). They are contained in Table VIII. There are small changes in $L(b$-axis) for PP(50), but all other L values appear to be insensitive to T_a for both TPE-PP samples.

The effect of the annealing temperature on melting behavior was studied. The sample was heated at 20 °C/min to 90 °C, held there for 5 min, cooled rapidly to ambient temperature, and annealed at different T_a for 12 h, and DSC was recorded at a 20 °C/min heating rate. The PP-

Table VIII
X-ray Diffraction Results[a]

	PP(25)		PP(50)		
	T_a = 30 °C	T_a = 45 °C	T_a = 30 °C	T_a = 45 °C	T_a = 60 °C
X_c, %	26	27	27 (30)	30	26 (25)
X_γ, %	69	70	58 (58)	61	65 (64)
$L(b$-axis), Å	50	49	67 (62)	56	40 (31)
$L(c$-axis), Å	40	44	38 (36)	41	40 (38)

[a] The samples were annealed at the indicated T_a for 24 h and cooled to room temperature, and X-ray diffraction was measured 24 h later, the results for which are given without parentheses. X-ray diffraction was also performed immediately after the sample and cooled from T_a to room temperature; the results are given in parentheses.

(0) material exhibits no melting endotherm. The melting behaviors of the other polymers are complicated as shown in Figure 17 and Table IX. There are two prominent peaks labeled P_1 and P_2 for crystalline phases melting at $T_{m,1}$ and $T_{m,2}$, respectively. An increase of T_a resulted in a significant increase of $T_{m,1}$ of about 10 °C for each 10 °C increment of T_a. $T_{m,1}$ approaches a limiting value of 68 °C for PP(50) annealed at 45 °C. A similar but smaller increase of $T_{m,2}$ with T_a was also observed. In addition, P_1 intensified at the expense of P_2. These transitions have low ΔH_f values of between 3 and 4 cal g^{-1}. An unexpected trend is that ΔH_f tends to decrease with the increase of T_a (columns 5 and 9 of Table IX). This trend parallels the effect of annealing on X_α ($=1 - X_\gamma$) and L found by X-ray diffraction (Table VIII). This may be explained by the fact that either the α-phase or larger size crystallites have higher ΔH_f than the γ-phase or smaller crystallites. There was a weak shoulder, P_3, in the DSC curves of PP annealed at $T_a < 25$ °C. This transition did not change appreciably with T_a but became indistinct for $T_a \geq 30$ °C.

The above melting behaviors are probably not due to the melting of the P_1 phase and recrystallizing into the P_2 phase. Because in this case $T_{m,2}$ should remain relatively independent of T_a. Since the α-phase of i-PP has much higher $T_{m,\alpha}$ for the α-phase than the $T_{m,\gamma}$ for the γ-phase, we might assume P_1 and P_2 to correspond to defective α- and γ-phases, respectively. X-ray diffraction showed the former to decrease with increasing T_a (Table VIII). The effect of annealing is probably related to the equilibrium melting phenomenon. The T_m would depend on T_a according to[22]

$$T_m = [T_m^\circ(2\beta - 1) + T_a]/2\beta \qquad (7)$$

where β indicates the fold length in multiples of the primary homogeneous nucleus, and T_m° is the equilibrium melting temperature obtained by extrapolating the data to $T_m = T_a = T_m^\circ$ (Figure 18). The results of P_2 led to $T_m^\circ = 102$ °C and $\beta = 0.94$ for PP(25) and $T_m^\circ = 104$ °C and $\beta = 0.94$ for PP(50). This extrapolation was over a large temperature range and cannot be taken as proof of the process. In the case of P_1, $T_{m,1}$ does not vary linearly with T_a; i.e., eq 7 does not apply. This may be rationalized by the assumption[4b] that those macromolecules containing frequent inversions of the chain configuration preferred to crystallize in the γ-modification; its nucleation and/or crystallization processes are more sensitive to T_a than the α-phase. It is assumed tacitly that in the use of eq 7 crystal thickening does not occur doing the DSC experiment, which may be untrue.

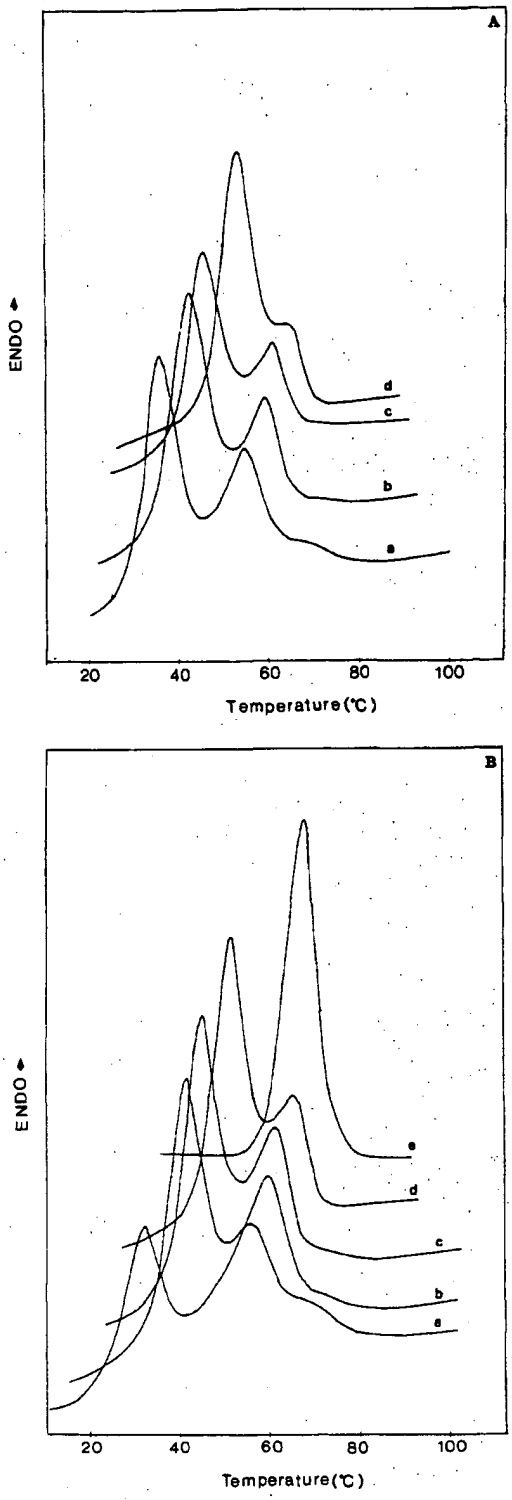

Figure 17. DSC curves: (A) PP(25) annealed at (top to bottom) 30, 25, 20, and 12 °C; (B) PP(50) annealed at (top to bottom) 45, 30, 25, 20, and 12 °C.

Discussion of the Results

Microstructures of TPE-PP. All the *ansa*-PP produced by 1 or 2 activated by MAO are waxy substances which contain acetone, diethyl ether, C_5, and soluble materials, and at low T_p polymers soluble in C_6 and C_7 and insoluble in C_7 were formed.[4] This indicates a broad range of polymer MW and stereoirregularity. In contrast PP(25) and PP(50) produced by 3/MAO are completely soluble in a single solvent and also have very low polydispersities (Table V). Therefore, these materials are uniform in both MW and microstructure. They exhibit characteristic properties of network elastomers: (a) the stress relaxation shows an equilibrium modulus, (b) the storage modulus shows a low-frequency plateau, (c) the tensile stress curve does not have a yield point, and (d) there is high elastic recovery. The fact that the polymer became a simple liquid above T_m indicates the physical cross-links are due to crystalline domains in these microphase-separated systems. Therefore, these materials are TPE and must have the stereoblock copolymer structure of $[(\text{cry-PP})_c(\text{am-PP})_a]_n$.

It is a difficult task to precisely determine the average block lengths a and c and number of blocks n in the present TPE containing a single monomer. We have attempted to obtain estimates for them.

The number-average molecular weights of the stereoirregular, noncrystallizable sequences between the crystallizable cross-links were estimated by the relationship of the rubber elasticity theory

$$\bar{M}_{n,a} = \rho RT/G_e \tag{8}$$

In this equation, ρ is the polymer density (900 kg m^{-3}), R is the gas constant (8.3 N m^3 K^{-1}), and T is the absolute temperature. The approximate $\bar{M}_{n,a}$ values were estimated to be 2100 and 4400 for PP(50) and PP(25), respectively, corresponding to a values equal to 50 and 105 for $(\text{am-PP})_a$. The total number of crystallizable propylene units in the average macromolecule is $X_c\overline{DP}_n$, where $\overline{DP}_n$ was obtained with GPC. The values of n and c can then be obtained readily from

$$n = \overline{DP}_n(1 - X_c)/a \tag{9}$$

and

$$c = X_c\overline{DP}_n/n \tag{10}$$

The structure of PP(25) is thus estimated to be $[(\text{am-PP})_{50}(\text{cry-PP})_{20}]_{30}$; it is $[(\text{am-PP})_{100}(\text{cry-PP})_{50}]_{10}$ for PP(50). The former has about 3 times as many blocks, but each block is about half the length of those in the latter.

The estimated c and a values have uncertainties intrinsic to TPE because of diffuse phase boundaries. This interphase mixing may be more problematical for the present TPE-PP than other TPE's such as polyurethanes and kratons. In the latter systems, the different domains are comprised of chemically dissimilar constituents and should have relatively sharp phase boundaries. In the TPE-PP, the amorphous segment may have x monomer units at both ends which are found in the diffuse phase boundaries, while the stereoregular segment may contain y monomer units at its termini similarly located. The macromolecular chain structure is closer to $[(\text{am-PP})_{a+2x}(\text{cry-PP})_{c-2y}]_{n'}$ than $[(\text{am-PP})_a(\text{cry-PP})_c]_n$. The approximate relationship is $n' \approx n(a + c)/(a + c + 2x - 2y)$. The important consequence is that $2y$ monomer units in the stereoregular segments do not crystallize.

A second source of uncertainty is due to extending the usage of eq 8, which was intended to estimate the MW of segments between ideal point cross-links. The application of eq 8 to systems with cross-links which are large crystalline domains may introduce an error on the order of $(2x + 2y)/n$. We are performing detailed analyses of 400-MHz ^{13}C NMR spectra for heptad steric sequence distributions and hope to obtain independent estimates for a, c, n, and x. In view of the above considerations, the absolute values of these quantities are rather uncertain,

Table IX
DSC Melting Behaviors of PP

	PP(25)				PP(50)			
	melting temp, °C				melting temp, °C			
sample T_c, °C	P_1	P_2	P_3	ΔH_f, cal/g	P_1	P_2	P_3	ΔH_f, cal/g
12	35.5	54.7	67.7	4.1	31.6	55.4	68.7	4.2
20	41.2	58.8	67.6	3.8	41.2	58.6	70.8	4.0
25	45.3	60.5	68.5	3.7	44.6	61.0	70.8	3.9
30	53.1	63.8	nd[a]	2.9	51.2	66.0	nd[a]	3.3
45					68.0	nd[a]	nd[a]	2.7

[a] Not detected due to overlapping or weak intensity.

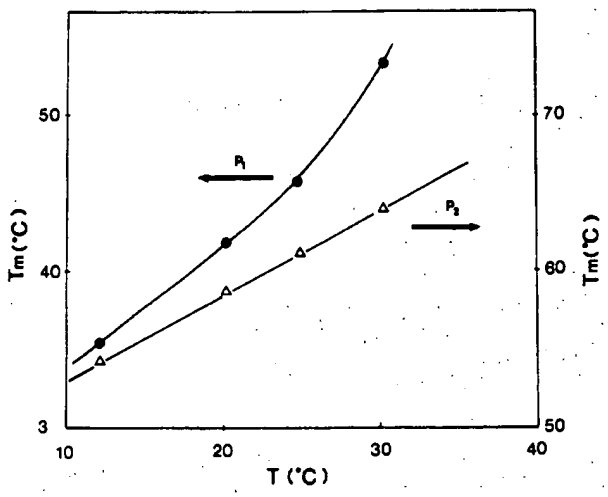

Figure 18. Variation of T_m with T_c according to eq 7.

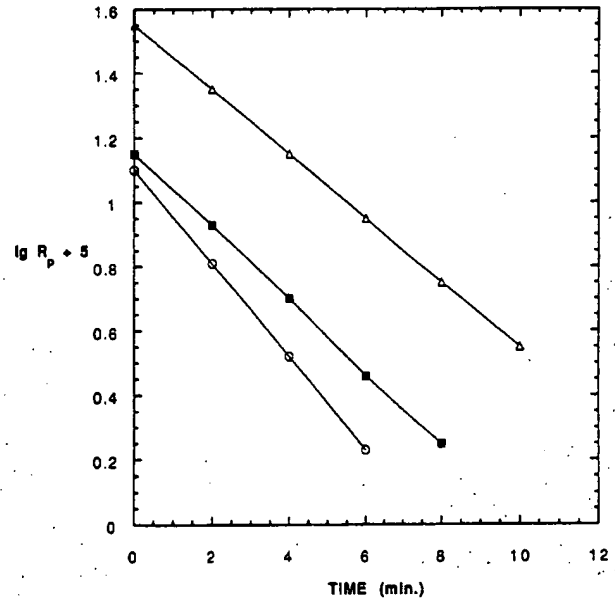

Figure 19. Variation of R_p versus t_p for the polymerizations in Figure 1; the symbols are the same.

but the relative values for TPE-PP's obtained at different T_p are meaningful. The effect of temperature on the extent of mixing at the phase boundary appears to be small since the X_c is insensitive to the annealing temperature (Table VIII).

It is noteworthy that the TPE-PP contains a high γ crystalline phase and that X_γ tends to increase with T_a. In other words, the γ-modification in this material is thermally stable like in aniso-PP (vide supra). This can be rationalized by nonconservation of helical configurations of neighboring crystallizable segments.

In the case of PP(25) the crystallizable segment corresponds to six 3/1 helixes for a length of 40 Å; this is not far from the observed crystallite size of ca. 42 Å in the c-dimension. On the other hand, the 46 monomer units in the crystallizable segment of PP(50) would have a length of ca. 100 Å, which is more than twice the maximum crystallite size. This may be explained by the presence of either insertion errors in the sequence or chain folding.

Our TPE-PP is entirely different from the elastomeric PP, which is of an in situ blend of i-PP and a-PP, reported and patented by Tullock and co-wokers.[23] These authors prepared the blend by polymerizing propylene with catalysts consisting of monohapto, trihapto, and hexahapto complexes of group IV elements supported on alumina. Typically the polymer obtained with the tetraneophylzirconium/Al_2O_3 catalyst is comprised of 50% of the heptane-insoluble material with $\bar{M}_n = 4.55 \times 10^5$ (PD = 5.8), 17.9% of the heptane-soluble fraction with $\bar{M}_n = 3.93 \times 10^4$ (PD = 23.9), and 28.2% of the ether-soluble polymer with $\bar{M}_n = 8.08 \times 10^4$ (PD = 7.5). The ether-soluble material is not elastic. The total polymer has an elastic recovery of only 7% after 300% elongation (i.e., a 93% permanent set). The authors considered the ether-soluble fraction to be the key component responsible for the elastic behavior of the blend. It was proposed that the ether fraction ([m m m m] ≈ 0.16–0.19) can cocrystallize with the isotactic heptane-insoluble fraction ([m m m m] ≈ 0.74) to form a cross-linked network. The heterogeneity of the Du Pont polymer was said to be due to the different kinds of active species formed by the reactions of the organometallic compounds with various types of surface hydroxyls of alumina.

Kinetics. Only a small fraction of 3 was converted to the active species by MAO. Furthermore, radio labeling found $[C^*]_0 = 3.9 \pm 0.2\%$ of 3 (Table II) at T_p from −20 to +25 °C. These results showed that the rates of formation of C^* and its deactivation have similar temperature dependences.

The R_p in Figure 2 increases significantly with the decrease of temperature. This is attributable to the higher solubility of propylene in toluene at lower T_p. Consequently, the values of k_p calculated from eq 1 are about 270 ± 80 $(M\ s)^{-1}$ between −20 and +25 °C. The measurement error for $R_{p,m}$ is large because of the rapid rise and decay of R_p.

The value of k_{tr}^A for chain transfer between Ti–P and MAO is $1.5 \times 10^{-2}\ s^{-1}$ at +25 °C, which decreases to $4 \times 10^{-3}\ s^{-1}$ at −20 °C.

The kinetics of propylene polymerization catalyzed by 1/MAO had been previously investigated.[4c] At T_p = 30 °C and [Al]/[Zr] = 3500, it was found that k_p = 970 $(M\ s)^{-1}$ and $k_{tr}^A = 0.015\ s^{-1}$. These values are similar to those given in Table II at 25 °C. However, there is a large decay of R_p for 3/MAO but not in the 1/MAO–Zr system. The data of Figure 2 are replotted in Figure 19 for log R_p versus

t_p. From the slopes of the straight lines we obtained the rate constant of deactivation (k_d). This value decreased from 5.7×10^{-3} s^{-1} at 25 °C to 3.8×10^{-3} s^{-1} at −20 °C. An Arrhenius plot of the data yielded a very small activation energy (<0.7 kcal mol^{-1}).

We have previously conducted an electron paramagnetic resonance (EPR) investigation of the reduction of Cp*TiCl$_3$ (Cp* = η^5-pentamethylcyclopentadienyl) by MAO.[24] When the two compounds were mixed at an Al/Ti ratio of 239 at −78 °C and brought up to room temperature, there was immediate alkylation and reduction of Cp*TiCl$_3$ as shown by visible and EPR spectra. Several Ti^{3+} species were formed, four of which were identified by EPR. Some of these species change with time. The dominant reduction product, which did not react further, was identified as η^3:η^4-(1,2,3-trimethyl-4,5-dimethylenecyclopentadienyl)-hydridotitanium(III). This reaction is not possible for the unsubstituted Cp and indenyl complexes. This difference may explain the more rapid reduction of the 3/MAO than the 1/MAO system. However, the reactions are too complicated for the kinetic order of the rate-determining step to be determined.

The MW of the PP was dependent on

$$\overline{DP}_n = \frac{k_p[m]}{k_d + k_{tr}^{A} + k_{tr}^{\beta}} \qquad (11)$$

From the values of k_p, [m], k_d, and k_{tr}^A (Table II), the $\overline{DP}_n$ should be about twice those found (Table V). Therefore, β-hydride elimination (rate constant = k_{tr}^{β}) is the chain-limiting process as has been shown for all homogeneous catalysts. The estimated values of k_{tr}^{β} are given in column 6 of Table II in parentheses. They are 3–10 times greater than k_{tr}^A.

At T_p = 50 °C, the PP MW is not appreciably dependent on t_p. At lower T_p there is a significant increase of MW with t_p. This suggests that the rates of chain transfer and deactivation decrease with the decrease of T_p, whereas the k_p value actually increases slightly (Table II). Both the MW and PD of PP increase as the results. Consequently PP(0) and PP(−20) contain polymers insoluble in diethyl ether but soluble in higher boiling aliphatic hydrocarbon solvents (Table IV).

State (Isomeric)-Switching Propagation. The formation of low-tacticity i-PP was usually attributed to steric insertion errors.[3,4] There may be present in the TPE-PP chain a few isotactic sequences of appreciable length for crystallization. This can be shown to be insignificant. By using a second-order Markov statistical analysis,[25] similar to that employed by Tullock and co-workers,[23] of the ^{13}C NMR spectra of the present TPE-PP,[10] we estimated about 10% of the monomer may be part of isotactic sequences of 16 units or longer. It was pointed out above that a few monomer units in each isotactic sequence are probably located in diffuse phase boundaries and are consequently not crystallized. Then a reasonable assumption is that only isotactic sequences longer than 21 propylene units will be crystallized. The probability of this occurrence was estimated to be less than 4% of the PP. The actual magnitude of X_c (Table VIII) is 26–30%. Therefore, the distribution of homosteric sequences must be nonrandom.

Nonrandom distribution of steric errors can result if there exist separate distinct catalytic species differing in stereoselectivity. This is the case for the catalysts which produce the in-situ blends reported by Tullock and co-workers.[23] However, the TPE-PP's of this work are characterized by narrow MW distribution and uniform solubility, indicating a homogeneous substance.

Another novel aspect of the present catalyst system is the variation of its stereospecificity with T_p. All previous heterogeneous Ziegler–Natta catalysts and homogeneous *ansa*-metallocene catalysts have increased stereospecificity at lower T_p. This is also true for the MAO-free "cationlike" system, [Et[Ind]$_2$Zr(CH$_3$)]$^+$[B(C$_6$F$_5$)$_4$]$^-$.[26] In contradiction, the stereospecificity of 3/MAO apparently *decreases* with the decrease of T_p so that PP(0) and PP(−20) are both devoid of crystallinity.

That the TPE-PP of this work contains alternating crystallizable and noncrystallizable segments in each macromolecular chain cannot be refuted. The simplest mechanism, which can explain the formation of such macromolecular structure is that a single active species can exist in two catalytic states which share the same k_p/k_{tr} ratio for polymerization but differ markedly in stereoselectivity. One state (3a) catalyzes nonstereoselective polymerization to form stereoirregular PP segments with a rate constant $k_{p,a}$; the other state (3c) promotes stereoselective monomer insertion to produce a $k_{p,c}$ stereoregular PP sequences. Furthermore, 3a and 3c interconvert at rate constants k_1 and k_{-1} at a time scale shorter than the kinetic chain lifetime

$$(\text{am-PP})_a \xleftarrow[k_{p,a}]{C_3H_6} \mathbf{3a} \underset{k_{-1}}{\overset{k_1}{\rightleftarrows}} \mathbf{3c} \xrightarrow[k_{p,c}]{C_3H_6} (\text{cry-PP})_c \qquad (12)$$

The relative rate of monomer incorporation into the am-PP and cry-PP blocks is

$$\frac{d[m_a]}{d[m_c]} = \frac{k_{p,a}[m][3a]}{k_{p,c}[m][3c]} \qquad (13)$$

where [m] is the propylene concentration. The $\overline{DP}_n$ is determined by

$$\overline{DP}_n = \frac{k_{p,a}[m][3a] + k_{p,c}[m][3c]}{k_d[3] + R_{tr,a} + R_{tr,c}} \qquad (14)$$

where R_{tr}'s are the rates of chain-transfer processes (vide supra). The copolymer block lengths are simply, $a = k_{p,a}[m]/k_1$ and $c = k_{p,c}[m]/k_{-1}$.

The PP's obtained at 0 °C or lower exhibit no crystallinity. This can be explained as the following. The values of $k_{p,a}/k_1$ are 400 and 110 at T_p = 50 and 25 °C, respectively. The approximate $\Delta E_{p,a} - \Delta E_1 \sim 4.5$ kcal mol^{-1}, which gives an estimate of $k_{p,a}/k_1 \sim 22$ M^{-1} or $a \sim 16$ at 0 °C. Similarly, the crystalline segment has $\Delta E_{p,c} - \Delta E_{-1} \sim 4.6$ kcal mol^{-1}, $k_{p,c}/k_{-1} \sim 10$ M^{-1}, and $c \sim 7$ at 0 °C. With the GPC $\bar{M}_n = 10^5$ (Table V) the approximate molecular structure of PP(0) is [(am-PP)$_{16}$(cry-PP)$_7$]$_{100}$. The cry-PP segment of only seven is too short to be crystallized. The rate constant ratio of propagation to state switching determines whether PP with TPE properties are produced or not, and $k_{p,c}[m]/k_{-1}$ should be greater than 20.

There are several possibilities for the structural differences between 3a and 3c. Since no TPE-PP has been obtained so far with the symmetric *ansa*-metallocene complexes, one may postulate at this point of time that the existence of isomeric states having different stereoselectivities is uniquely associated with the nonsymmetric *ansa*-hapto ligand. In the case of the dimethyl derivative 6, the ^1H NMR chemical shifts of the two methyl singlet resonances were found at −1.09 and +0.17 ppm.[14] X-ray structure showed one methyl group to be situated proximal to the indenyl ring and the other to the tetramethylcyclopentadienyl ring. These methyl groups, and consequently the propagating Ti–P groups, are endowed with different steric environments and may produce alternate blocks of crystallizable and noncrystallizable PP

segments leading to TPE-PP.

Conclusions. We have synthesized the nonsymmetric *ansa*-titanocene compound 3. When activated by MAO, it can produce PP possessing interesting and useful properties. PP(25) and PP(50) are soluble in a single solvent and have MWD ~ 1.7–1.9. Morphologically they contain ca. 30% crystallinity of which about two-thirds is present in the γ-modification. Rheologically, the G^*, G', and G'' decay sharply at T_m; they became frequency independent below T_m and decrease monotonically with the increase of frequency above T_m. The materials do not display a yield point, possess very high elongations to break, and exhibit excellent elastic strain recoveries. These properties are those of a thermoplastic elastomer with crystalline domains acting as network cross-links. A mechanism of polymerization was postulated invoking an active species having two interconverting propagating states which catalyze the formation of alternating stereoregular/crystallizable and stereoirregular/amorphous segments. This suggests that *ansa*-metallocene complexes are fluxional rather than stereorigid at the time scale between 10- and 100-fold of the turn over time, i.e., 0.2–2 s.

Acknowledgment. G.H.L. is the recipient of a postdoctoral fellowship from the Ministerio de Education y Ciencia (Spain).

References and Notes

(1) *Homogeneous Ziegler–Natta Catalysts.* Part 1: Chien, J. C. W.; Wang, B. P. *J. Polym. Sci., Part A* **1988**, *26*, 3089. Part 17: Salajka, Z.; Dong, S.-H.; Chien, J. C. W., submitted for publication in *J. Polym. Sci., Part A.*

(2) (a) Department of Polymer Science and Engineering. (b) Department of Chemistry. (c) Department of Chemical Engineering.

(3) Ewen, J. A. *J. Am. Chem. Soc.* **1984**, *106*, 6355.

(4) (a) Rieger, B.; Chien, J. C. W. *Polym. Bull.* **1989**, *21*, 1959. (b) Rieger, B.; Mu, X.; Mallin, D. T.; Rausch, M. D.; Chien, J. C. W. *Macromolecules* **1990**, *23*, 3559. (c) Chien, J. C. W.; Sugimoto, R. *J. Polym. Sci., Part A* **1991**, *29*, 459. Professor T. Atkins of Bristol University recommended the usage of the Greek prefix "an" to describe structures that deviate away from a limiting ordered structure.

(5) (a) Kaminsky, W.; Külper, K.; Brintzinger, H. H.; Wild, F. R. W. P. *Angew. Chem.* **1985**, *97*, 507. (b) Kaminsky, W. *Angew. Chem., Makromol. Chem.* **1986**, *145/146*, 149. (c) Kaminsky, W. *Catalytic Polymerization of Olefins*; Keii, T., Soga, K., Eds.; Kodansha Elsevier: Tokyo, 1986; p 293.

(6) Ewen, J. A. *Catalytic Polymerization of Olefins*; Keii, T., Soga, K., Eds.; Kodansha Elsevier: Tokyo, 1986; p 271.

(7) Hanson, K. R. *J. Am. Chem. Soc.* **1966**, *88*, 2731.

(8) Kaminsky et al.[6a,b] reported that less than 1% of the PP was soluble in toluene but did not specify the solubility conditions.

(9) Some reports regarding the γ-modification of polypropylene and the $\gamma \rightarrow \alpha$ transformation are as follows: (a) Pae, K. D.; Morrow, D. R.; Sauer, J. A. *Nature* **1966**, *211*, 514. (b) Kardoss, J.; Christiansen, A. W.; Baer, E. *J. Polym. Sci., Polym. Phys. Ed.* **1968**, *4*, 777. (c) Pae, K. D. *J. Polym. Sci., Polym. Phys. Ed.* **1968**, *6*, 657. (d) Lotz, B.; Graff, S.; Wittmann, J. C. *J. Polym. Sci., Polym. Phys. Ed.* **1986**, *24*, 2017. (e) Morrow, D. R.; Newman, B. Z. *J. Appl. Phys.* **1968**, *39*, 4944. (f) Krestev, V. P.; Dobreva, B.; Atanasov, A. M.; Nedkov, E. T. *Morphology Polymers*; W. de Gruyter & Co.: Berlin, 1986; p 303. (g) Addink, E. J.; Beintema, J. *Polymer* **1961**, *2*, 185. (h) Turner-Jones, A.; Aizlewood, J. M.; Beckett, D. R. *Makromol. Chem.* **1964**, *75*, 134. (i) Corradini, P.; Petraccone, V.; Pirozzi, B. *Eur. Polym. J.* **1983**, *19*, 249. (j) Kojima, M. *J. Polym. Sci., Polym. Phys. Ed.* **1968**, *6*, 1255.

(10) Mallin, D. T.; Rausch, M. D.; Lin, Y.-G.; Dong, S.-H.; Chien, J. C. W. *J. Am. Chem. Soc.* **1990**, *112*, 2030.

(11) TPE is a phase-separated block copolymer characterized by rigid or crystalline domains which act as physical cross-links below T_g or T_m, respectively, for the soft or amorphous domains.

(12) Pervin, D. D.; Armarego, W. L. F. *Purification of Laboratory Chemicals*, 2nd ed.; Pergamon Press, Ltd.: London, 1980.

(13) Bensley, D. M.; Hintz, E. A. *J. Organomet. Chem.* **1988**, *353*, 93.

(14) Chien, J. C. W.; Llinas, G. H.; Rausch, M. D.; Lin, Y.-G.; Winter, H. H.; Atwood, J. L.; Bott, S. G. *J. Am. Chem. Soc.* **1991**, *113*, 8569.

(15) Chien, J. C. W.; Kuo, C. J.; Ang, T. *J. Polym. Sci., Polym. Chem. Ed.* **1985**, *23*, 723.

(16) (a) Chien, J. C. W.; Kuo, C. I. *J. Polym. Sci., Polym. Chem. Ed.* **1985**, *23*, 731. (b) Schen, M. A.; Karasz, F. E.; Chien, J. C. W. *J. Polym. Sci., Polym. Chem. Ed.* **1983**, *21*, 2787. (c) Chien, J. C. W.; Wang, B. P. *J. Polym. Sci., Polym. Chem. Ed.* **1988**, *26*, 3089. (d) Chien, J. C. W.; Hu, Y. *J. Polym. Sci., Polym. Chem. Ed.* **1987**, *25*, 2881. (e) Chien, J. C. W.; Wang, B. P. *J. Polym. Sci. Part A* **1989**, *27*, 1539; **1990**, *28*, 15. (f) Chien, J. C. W.; Zhou, X. H.; Lin, S. *J. Polym. Sci., Part A* **1990**, *28*, 2609.

(17) Chiang, R. *J. Polym. Sci.* **1957**, *28*, 235.

(18) Pasquon, I. *Pure Appl. Chem.* **1967**, *15*, 465.

(19) Time–temperature superposition. Curves $G'(\omega)$ and $G''(\omega)$ measured at different temperatures can be superposed by shifting along the frequency axis by temperature shift factor a_T, i.e., $G'(a_T\omega,T) = G'(\omega_0,T_0)$ and $G''(a_T\omega,T) = G''(\omega_0,T_0)$, where ω_0 is the reduced frequency and T_0 is the reference temperature. Time–temperature superposition does not apply to a temperature range which involves any kind of phase transition.

(20) Lin, Y.-G.; Mallin, D. T.; Chien, J. C. W.; Winter, H. H. *Macromolecules* **1991**, *24*, 850.

(21) (a) Alexander, L. E. *X-ray Diffraction in Polymer Science*; John Wiley and Sons, Inc.: New York, 1969. (b) Dong, S.-H. *Acta Polym. Sin.* **1987**, *2*, 119.

(22) Hoffman, J. D.; Weeks, J. J. *J. Res. Natl. Bureau Stand.* **1962**, *66A*, 13.

(23) (a) Tullock, C. W.; Tebbe, F. N.; Mulhaupt, R.; Overnall, D. W.; Setterquist, R. A.; Ittel, S. D. *J. Polym. Sci., Part A* **1989**, *27*, 3063. (b) Collette, J. W.; Tullock, C. W.; MacDonald, R. N.; Buck, W. H.; Su, A. C. L.; Harrell, J. R.; Mulhaupt, R.; Anderson, B. C. *Macromolecules* **1989**, *22*, 3851. (c) Tullock, C. W.; Mulhaupt, R.; Ittel, S. D. *Macromol. Chem., Rapid Commun.* **1989**, *10*, 19.

(24) Bueschges, U.; Chien, J. C. W. *J. Polym. Sci., Part A* **1989**, *27*, 1525.

(25) Mallin, D. T. Ph.D. Dissertation, University of Massachusetts, Amherst, MA, 1991.

(26) Chien, J. C. W.; Tsai, W.-M.; Rausch, M. D. *J. Am. Chem. Soc.* **1991**, *113*, 8570.